Remaining Useful Life Prediction of Rolling Bearings Based on Segmented Relative Phase Space Warping and Particle Filter

Hengyu Liu, Rui Yuan, *Member, IEEE*, Yong Lv, Hewenxuan Li, Ersegun Deniz Gedikli, and Gangbing Song, *Member, IEEE*

***Abstract*— Predictive maintenance plays a crucial role in the field of intelligent machinery fault diagnosis, which improves the efficiency of maintenance. This article focuses on the extraction of real-time damage feature and the prediction of remaining useful life (RUL) in predictive maintenance of rolling bearings. Some RUL prediction approaches lack dynamic foundations and require large amounts of data and prior knowledge. This article proposes the algorithm of segmented relative phase space warping (SRPSW) and a strategy combining double exponential model (DEM) and particle filter (PF) to predict the RUL. SRPSW provides a dynamic basis for real-time RUL prediction in different stages. The DEM-based PF reduces the need for prior knowledge and improves the accuracy. The analysis results from normal and accelerated degradation experiments show that the proposed SRPSW overcomes the failure of the original PSW in depicting the later operating stage of bearings. Further, the relative damage indicators (RDIs) extracted by SRPSW are more accurate than commonly used indicators. The predicted results show that the DEM-based PF does not require professional and prior information while ensuring the accuracy of RUL prediction. The proposed approach in this article provides a new avenue for predictive maintenance of bearings.**

***Index Terms*— Particle filter (PF), remaining useful life (RUL) prediction, rolling bearing degradation, segmented relative phase space warping (SRPSW).**

Manuscript received 10 July 2022; revised 9 September 2022; accepted 4 October 2022. Date of publication 13 October 2022; date of current version 1 November 2022. This work was supported in part by the National Natural Science Foundation of China under Grant 51875416, in part by the Natural Science Foundation Innovation Group Program of Hubei Province under Grant 2020CFA033, and in part by China Postdoctoral Science Foundation under Grant 2020M682492. The Associate Editor coordinating the review process was Kristen M. Donnell. *(Corresponding author: Rui Yuan.)*

Hengyu Liu, Rui Yuan, and Yong Lv are with the Key Laboratory of Metallurgical Equipment and Control Technology, Ministry of Education, and the Hubei Key Laboratory of Mechanical Transmission and Manufacturing Engineering, Wuhan University of Science and Technology, Wuhan 430081, China (e-mail: liuhengyu@wust.edu.cn; yuanrui@wust.edu.cn; lvyong@wust.edu.cn).

Hewenxuan Li is with the Department of Mechanical, Industrial and Systems Engineering, University of Rhode Island, Kingston, RI 02881 USA (e-mail: hewenxuan_li@uri.edu).

Ersegun Deniz Gedikli is with the Department of Ocean and Resources Engineering, University of Hawaii at Manoa, Honolulu, HI 96822 USA (e-mail: egedikli@hawaii.edu).

Gangbing Song is with the Smart Materials and Structures Laboratory, Department of Mechanical Engineering, University of Houston, Houston, TX 77204 USA (e-mail: gsong@uh.edu).

Digital Object Identifier 10.1109/TIM.2022.3214623

I. Introduction

IN THE field of mechanical engineering, signal processing-based maintenance and prognostics have drawn extensive attentions. The maintenance strategies have been developed from periodic maintenance to predictive maintenance [1], [2]. As key components in modern machinery, bearings often operate at high speed with heavy loads and are exposed to harsh working conditions. These adverse factors may lead to bearing failures, resulting in economic loss and even casualty accident [3], [4], [5]. Therefore, the predictive maintenance of the bearings is of great importance. The features of the bearings can be extracted by traditional signal decomposition algorithms [6], [7], [8], [9], [10]. However, some of these methods cannot be effectively applied to predictive maintenance of the bearings.

Health monitoring is the key part in predictive maintenance of the bearings [11], [12]. The health degradation of bearings can be tracked from the analysis of the vibration signals, which are collected by acceleration sensors. The extracted degradation trends can be used to predict the remaining useful life (RUL) of the bearings. As a result, the failures are detected in advance and the machinery is maintained in a planned way. The health monitoring process consists of four steps: signal acquisition, construction of damage indicators (DIs), classification of damage stages, and RUL prediction [13]. As for the signal acquisition, vibration signal [14], acoustic emission signal [15], temperature signal [16], wear debris [17], and current signal [18] have been used to monitor bearing status, and vibration signals are most commonly used.

It should be noted that these bearing damages are hard to observe directly [19]; thus, DIs are usually extracted to show the damage process. Two types of DIs were specified by prior researches: virtual damage indicators (VDIs) and physics damage indicators (PDIs) [20]. VDIs usually have no physical meaning. The damage degradation trend is described virtually by the VDIs. In contrast, PDIs are related to the physical property of the damage. PDIs are usually extracted from the signals by statistical methods or signal processing methods, such as root-mean-square value [21] and spectral kurtosis [22]. Deep-learning-based approaches are widely applied in VDIs construction. Que et al. [23] employed an attention

mechanism to construct VDIs. The accuracy of VDIs is improved by combining the attention mechanism with dynamic time warping. Peng et al. [24] employed a deep belief network to extract hidden VDIs. Pan et al. [25] employed the relative root mean square as PDIs while improving extreme learning machines to achieve RUL prediction. This strategy improves the adaptability of DIs to different bearings and various working conditions. Wang et al. [26] employed relevance vector machine to extract DIs, and Pan et al. [27] defined the DIs as the obedience of the data to the normal working stage. Since the mechanism of bearing damage is complex and the existing VDIs lack of theoretical dynamical basis, it is difficult to interpret the relationship between DIs and the damage. Chelidze and Liu [28] proposed the algorithm of phase space warping (PSW), where the hierarchical dynamical system is constructed in a high-dimensional phase space. The curvatures of the trajectory in the phase space represent the dynamic property of the nonlinear system [29]; thus, the PDIs extracted by PSW are utilized in RUL prediction of faulty component. Luo et al. [30] further proposed an improved PSW algorithm by optimizing the selection of parameters to track the degradation of bearing. Qian et al. [31] optimized the algorithm of PSW by multidimensional auto-regression and employed a modified Paris model for RUL prediction. During the bearing degradation process, the amplitude of vibration signal increases along with the increase of degradation status correspondingly. This phenomenon causes a drastic change in the damage-phase-space trajectory.

As the last step in bearing prognostics, RUL prediction can be divided into three types: model-based methods, data-based methods, and hybrid methods [20]. Model-based methods mainly use mathematical models to describe the degradation process in RUL prediction [32]. Data-based methods mainly use empirical knowledge and statistical models to describe the degradation process [33]. Further, the statistical and physical models can be combined to form the hybrid model to conduct RUL prediction [34]. Deep-learning-based methods are well-applied for RUL prediction. Yan et al. [35] enhanced the long short-term memory network to improve the prediction accuracy and convergence speed. Wang et al. [36] proposed a deep separable convolutional network to make better use of the data collected by different sensors. Several model-based and hybrid methods also attract the interest of researchers. Wang and Xiang [37] employed an exponential model to simulate the bearing damage degradation process. In addition, Wang and Gao [38] combined the Paris model and Newman model to improve the accuracy of RUL prediction. These fatigue crack growth model-based methods require extensive knowledge of material parameters and fatigue mechanisms, thus making it difficult to achieve ideal RUL prediction with high efficiency.

In this article, a novel real-time segmented relative phase space warping (SRPSW) algorithm for rolling bearing RUL prediction is proposed. The indicators extracted by SRPSW are related to the dynamic characteristics of damage; hence, relative damage indicators (RDIs) are PDIs. The double exponential model (DEM) is combined with the particle filter (PF) algorithm to improve the accuracy of RUL prediction

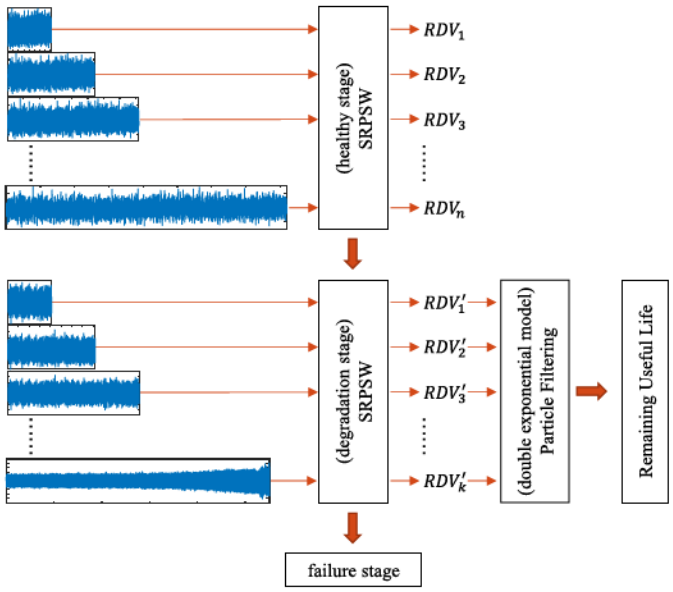

Fig. 1. Real-time RUL prediction process.

in SRPSW. PF adopts the SRPSW extracted RDIs as the prior information to predict the RUL. The use of DEM avoids the need for extensive prior knowledge of the damage itself. The rest of this article is organized as follows. Section II introduces the PSW algorithm and the proposed real-time SRPSW. Section III describes the establishment of the PF based on DEM. Section IV utilizes the laboratory datasets from run-to-failure test to verify the validity of the proposed approach. Section V concludes this article by drawing main conclusions and giving necessary discussions.

II. Segmented Relative Phase Space Warping

This article proposes a novel RUL prediction approach to rolling bearings based on the SRPSW and PF. SRPSW is proposed to extract RDIs, while damage stages are also divided specifically to improve the accuracy of damage tracking. The graphical illustration of the proposed approach in this article is shown in Fig. 1. First, the vibration signal of the bearing is collected. SRPSW is employed to extract RDIs, and the relative damage vectors (RDVs) are constructed by the extracted RDIs. Second, the determination about whether the extracted RDIs in RDV exceeds the threshold of the healthy stage is conducted. If RDIs exceed the threshold, the bearings degradation stage can be identified. Correspondingly, the parameters of SRPSW are reselected to avoid errors. Finally, the RDVs are adopted as the input to PF to achieve accurate and efficient RUL prediction of rolling bearing.

A. Theory of Phase Space Warping

As the basis of SRPSW, PSW extracts the slow-time variable in the dynamic system [39]. A hierarchical dynamical system is proposed. Luo et al. [30] clarifies that the damage and vibration of the bearing conform to the characteristics of a hierarchical dynamical system. The system is simplified to

a coupled state of fast-time variables (vibration signals) and slow-time variables (damage signals), defined as

$$\dot{x} = f(x, \mu(\phi), t) \tag{1}$$

$$\dot{\phi} = \varepsilon g(x, \phi, t) \tag{2}$$

$$s = h(x) \tag{3}$$

where $x \in \mathbb{R}^n$ is the fast-time variable; $\phi \in \mathbb{R}^m$ is the slow-time variable in damage evolution; $f(\cdot)$ and $g(\cdot)$ are the fast and slow dynamics functions; $\mu \in \mathbb{R}^s$ is the function of ϕ as a kind of parameter vector; t is the time; and $\varepsilon \in (0, 1]$ is a small ratio constant that distinguishes the time scale of fast and slow variables. s is the discrete time series collected by the sensor, and $h(\cdot)$ is the measure function for linking discrete time series and fast variables.

To track damages from vibration signals, a hierarchical dynamics system should be decoupled. The slow-time variables (e.g., damage variable) can be identified with the known fast-time vibration signals. Considering a single damage variable, the damage state is obtained after a short time interval t_p from the initial time t_0 and is described as

$$x(t_0 + t_p, \varepsilon) = F(x_0, t_0, t_p, \mu(\phi)) \tag{4}$$

where $F(\cdot)$ is the function of $\mu(\phi) \in \mathbb{R}^n$. Every different damage ϕ in fast subsystems with the same initial points is evaluated by $F(\mu(\phi))$. The damage process can be tracked through $\mu = F^{-1}(x) : \mathbb{R}^n \to \mathbb{R}^s$ or $\phi = F^{-1}(x) : \mathbb{R}^n \to \mathbb{R}^m$.

The reference state (healthy stage) obtained after the same time is $x(t_0 + t_p, \varepsilon)$. After Taylor series expansion at $x = x_0$ and $\phi = \phi_R$, (4) is written as

$$\begin{aligned} x(t_0 + t_p, \varepsilon) &= F(x_0, t_0, t_p, \mu(\phi)) \\ &= F(x_0, t_0, t_p, \mu(\phi_0)) + o(\varepsilon) \\ &= F(x_0, t_0, t_p, \mu(\phi_R)) + \frac{\partial x}{\partial \mu}\frac{\partial \mu}{\partial \phi}(\phi_0 - \phi_R) \\ &\quad + o(\|\phi_0 - \phi_R\|^2) + o(\varepsilon) \end{aligned} \tag{5}$$

where ϕ_0 represents the initial damage, ϕ_R is the reference damage, and $o(\cdot)$ represents the higher order infinitesimals.

The error between the damage state and the reference state, e_R, is used to track damage degradation

$$\begin{aligned} e_R &= F(x_0, t_0, t_p, \mu(\phi)) - F(x_0, t_0, t_p, \mu(\phi_R)) \\ &= \frac{\partial x}{\partial \mu}\frac{\partial \mu}{\partial \phi}(\phi_0 - \phi_R) + o(\|\phi_0 - \phi_R\|^2) + o(\varepsilon). \end{aligned} \tag{6}$$

Ignoring the high-order infinitesimals, the approximate error is as follows:

$$e_R \approx C(x_0, t_0, t_p, \phi_R)\phi + c(x_0, t_0, t_p, \phi_R) \tag{7}$$

where $C = (\partial x/\partial \mu)(\partial \mu/\partial \phi)$ and $c = -C\phi_R$. Equation (7) is applicable to any damage variable, and the subscript of damage variable ϕ_0 is removed. $\|\phi_0 - \phi_R\|^2$ and ε are small; hence, e_R and ϕ are approximately linear. Then, fast-time variables are applied to track the evolution of damage.

To quantify this error, SRPSW is divided into five steps, which are illustrated in Fig. 2.

Step 1: Vibration signals are collected in real time. The red dashed rectangles in Fig. 2(a) represent data segments collected at different times.

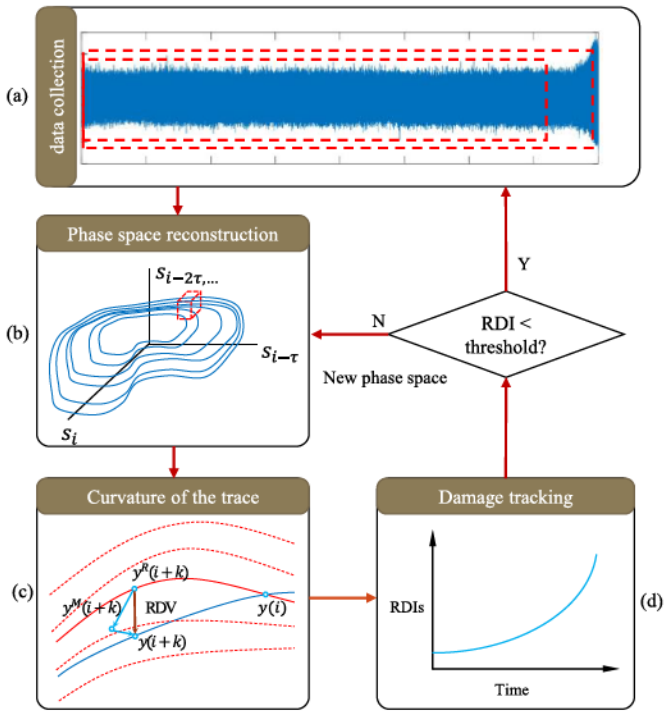

Fig. 2. Flowchart of SRPSW. (a) Time-domain signal. (b) Phase space reconstruction. (c) Local phase space. (d) Damage tracking.

Step 2: The signal of the bearing is embedded in the reconstructed phase space. Fig. 2(b) shows the trajectory of the signal being reconstructed into high-dimensional phase space. S_i refers to the axes of the phase space. The red dashed cube refers to a subspace in the phase space, and the warping of the phase trajectory is analyzed in this subspace.

Step 3: In Fig. 2(c), the blue solid line is the phase space trajectory in a short time interval t_p. $y(i)$ is the phase point at the current moment. The healthy reference phase space trajectory is the red solid line, and $y^R(i + k)$ is the point on the curve at the next instant. $y(i + k)$ is the phase point at the next moment, and $y^M(i + k)$ is the phase point at the next moment predicted by SRPSW. Damage causes the warping of phase space.

Step 4: RDIs were extracted from the RDV.

Step 5: The phase space is reconstructed if the RDI exceeds the threshold. If the RDI does not exceed the threshold, the signal continues to be collected.

Based on the Takens theorem [40], the time-delay approach is adopted to reconstruct the phase space of the vibration signal $\{s_i\}_{i=1}^N$ to generate a d-dimensional state vector

$$y(i) = [s_i, s_{i+\tau}, \ldots, s_{i+(d-1)\tau}]^T \tag{8}$$

where $\{s_i\}_{i=1}^N$ represents the time series of vibration signals, and $y(i)$ is the point in the reconstructed phase space. The embedding dimension d is determined by the false-nearest-neighbors method [41], and the time delay τ is estimated by the mutual information method [42]. The reconstructed reference phase space $y(i; \phi_R)$ is constructed in the same way. The map P describes the reconstructed state vector $y(i + 1) = P(y(i); \phi)$. After a short-time interval t_p from

time t_0, state point $y(i+k)$ is expressed as follows:

$$y(i+k) = P^k(y(i); \phi) \tag{9}$$

where k is the number of mapping interactions in t_p. A short-term linear prediction model is applied to construct the reference phase space, predicting the state of $i+k$ with the state point $y(i)$

$$y(i+k) = A_i^k y(i) + b_i^k \tag{10}$$

where A_i^k and b_i^k are the parameters of the linear prediction model at the ith point.

Since the prediction reference model is not perfect, the points $y_M(i+k)$ after k steps are considered. The true error is $E_k^R(i)$, the estimated error is $E_k(i)$, and the modeling error is $E_k^M(i)$

$$E_k^R(i) = y(i+k) - y^R(i+k) \tag{11}$$

$$E_k(i) = y(i+k) - y^M(i+k) \tag{12}$$

$$E_k^M(i+k) = y^M(i+k) - y^R(i+k). \tag{13}$$

The tracking matrix is expressed as

$$\begin{aligned} e_R(y(i); \phi) &= P(y(i); \phi) - P(y(i); \phi_R) \\ &\approx y(i+1) - A_i y(i) + b_i. \end{aligned} \tag{14}$$

The collected bearing vibration signal is divided into nr segments for phase space reconstruction, and nb independent subspaces $\{\mathcal{B}_i\}_{i=1}^{nb}$ are segmented. The accuracy of the results is improved by calculating the average error of the damage from the reference in each subspace. Therefore, the damage tracking function of the data segment is

$$c_i(\phi) = \frac{1}{N} \sum_{i=1}^{N} \|e_R(y(i); \phi)\| \tag{15}$$

where N is the number of damage space points in the subspace $\{\mathcal{B}_i\}_{i=1}^{nb}$, and the damage of all subspace is collected into an nb-dimensional vector

$$c^j = [c_1(\phi), c_2(\phi), \ldots, c_{nb}(\phi)]^T. \tag{16}$$

The damage vectors of all nr data segments are computed and then arranged to form a damage matrix in chronological order

$$Y = \left[c^1, c^2, \ldots, c^{nr}\right]. \tag{17}$$

B. Extraction of DIs With SRPSW

It should be noted that the trajectories exceed the bounds of the space where the warping is measured, resulting in nulls and invalidating the algorithm. Thus, the original algorithm of PSW is not entirely suitable for vibration signals of rolling bearings. The constructed reference phase space must meet the following conditions [43].

1) The effective dimension does not increase.
2) The future system phase space trajectory cannot exceed the reference phase space trajectory.

In the process of bearing degradation, the dynamic system changes greatly. Thus, the reference phase space may not contain all phase space trajectories, and the reference phase space may fail in the later working stage of bearing. In addition, the original PSW algorithm cannot track damage by stages. The result of PSW is a damage tracking matrix, which contains a lot of nonprimary damage information. This article uses the smooth orthogonal decomposition algorithm for reference [28]. To realize the real-time tracking of damage and extract the main damage information, the eigenvector with the largest smoothness is extracted as the main damage trend [44]. PSW uses different reconstructed phase spaces and reference phase spaces during the staged damage tracking; thus, the original algorithm cannot avoid the fluctuation of the indices extracted from damage in different stages.

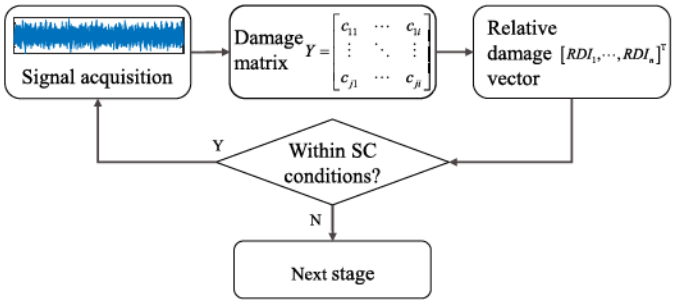

Fig. 3. Calculation process of SRPSW.

To resolve the problems of damage matrix error and segmental tracking indicator fluctuation, a real-time segmented relative vector tracking algorithm is proposed in SRPSW. The degradation threshold and failure threshold are determined by the condition of segmentation (3σ principle), and the degradation process of the bearing is divided into healthy stage, degradation stage, and failure stage. Since damage tracking metrics are converted to relative values, damage metrics is tracked in segments.

Fig. 3 illustrates the calculation process of the proposed SRPSW algorithm. The initial part of the signal is used to determine the parameters of the PSW. The damage matrix is extracted from the vibration signal, and the main RDV in the damage matrix is extracted by SRPSW. RDIs in RDV correlate to bearing damage. When RDI exceeds the segmentation conditions (SCs), the bearing enters the degradation stage, and new parameters are determined. Then, the same process is performed until the bearing enters the failure stage from the degradation stage.

The collected real-time bearing vibration signal is processed by PSW, and the damage tracking matrix Y is obtained. Conversion of the extraction of DIs into the extraction of eigenvalues leads to

$$\left[Y^T Y\right] q = \lambda \left[(DY)^T DY\right] q \tag{18}$$

where D is the discrete differential operator of the forward difference, q is the eigenvector, and λ is the corresponding eigenvalue. The eigenvector corresponding to the largest eigenvalue maximizes the smoothness of the mapping of the damage tracking matrix Y. The generalized singular value

decomposition is applied to solve (17)

$$\begin{aligned} Y &= UCX^{\mathrm{T}} \\ DY &= VSX^{\mathrm{T}} \\ C^{\mathrm{T}}C + S^{\mathrm{T}}S &= I \end{aligned} \tag{19}$$

where I is the identity matrix, U and V are the unitary matrices, X is a square matrix, and C, S are the nonnegative diagonal matrices. The eigenvalue is $\lambda_i = (C(i,i)/S(i,i))^2$, and the transformed tracking matrix is $\hat{Y} = UC$, whose column vectors are arranged in the descending order of eigenvalues; thus, the main damage feature is the first column of $\hat{Y}$. Due to different phase space states in different damage stages, the segmented RDI is expressed as

$$\mathrm{RDI}(i) = \frac{\mathrm{DI}(i) - \mathrm{DI}_m}{\mathrm{DI}_m} \tag{20}$$

where $\mathrm{DI}(i)$ is the damage feature, DI_m is the initial damage of the bearing at each stage, and the RDI at different stages are extracted by benchmark DI_m.

The bearing from the healthy stage to the degradation stage is classified using the 3σ interval. The 3σ principle was used to determine thresholds for RDIs during normal working stages [5]. The vibration signal for the normal operation of the bearing is disturbed, which causes fluctuations in the RDIs extracted from the signal. The mean value μ and standard deviation σ of the RDIs are computed. Mean and standard deviation are used to limit the range of RDIs, i.e., $[\mu - 3\sigma, \mu + 3\sigma]$. To ensure the robustness of the method, the bearing is considered to enter the degradation stage only when three consecutive RDIs exceed the interval. The failure threshold is artificially set at the later stage of the bearing degradation. When RDIs surpass the threshold, the bearing is deemed to have entered the failure stage. Currently, the bearing is still operational, but it was already defective.

C. Evaluation Criteria of DIs

To better understand the impact of the DIs proposed in this article, monotonicity is introduced as evaluation criterion [45], [46]. The damage evolution process of the bearing is one way. Thus, the monotonicity of the index reflects the effect of tracking damage. Monotonicity is calculated as [47]

$$M = \frac{1}{n-1}\sum_{i=1}^{n-1}\left[\mathrm{sgn}(x_{i+1} - x_i)\right] \tag{21}$$

where M is the monotonicity value, n is the total number of the DIs of the bearing, x_i is the ith DI of the bearing, and $\mathrm{sgn}(\cdot)$ is the signum function expressed as

$$\mathrm{sgn}(x) = \begin{cases} 1 & x > 0 \\ 0 & x = 0 \\ -1 & x < 0. \end{cases} \tag{22}$$

The experimental part will discuss the monotonicity of the proposed DI compared with the traditional PDIs. The DIs used for comparison are shown in Table I.

TABLE I
PDIs FOR COMPARISON

PDIs	Definition
Root mean square	$\sqrt{\frac{1}{N}\sum_{i=1}^{N}\lvert x_i\rvert^2}$
Standard deviation	$\sqrt{\frac{1}{N-1}\sum_{i=1}^{N}\lvert A_i-\mu\rvert^2}$
Kurtosis	$\frac{1}{N}\sum_{i=1}^{N}\frac{(x_i-\mu_x)^4}{\sigma_x^4}$
Skewness	$\frac{1}{N}\sum_{i=1}^{N}\frac{(x_i-\mu_x)^3}{\sigma_x^3}$
Permutation Entropy	$H_{pe}(m) = -\sum_{m!} P\log(P)$
Peak to Peak	Maximum-to-minimum difference

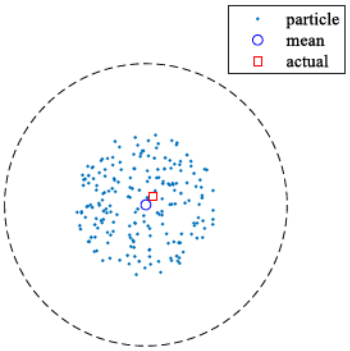

Fig. 4. Schematic of the PF.

III. PF AND RUL PREDICTION

A. Theory of DEM-Based PF

PF is an approximation algorithm based on Monte Carlo simulation [48]. As shown in Fig. 4, the PF algorithm approximates the model parameters by computing the mean of the particle set. The heart of the algorithm is to approximate the probability density function of the model variables. The integral operation with the sample mean is then replaced, and the parameters are estimated by minimizing the variance.

In this article, a DEM is applied to simulate the bearing degradation process. PF algorithm estimates the model parameters and predicts the RUL. The system is described in the form of state and observation equations as

$$\begin{cases} X(k) = p(X(k-1), W(k)) \\ Z(k) = h(X(k), V(k)) \end{cases} \tag{23}$$

where $X(k)$ and $X(k-1)$, respectively, represent the state of the system at k and $k-1$. $Z(k)$ represents the measurement data at time k. $W(k)$ is the process noise of the system, and $V(k)$ is the measurement noise of the sensors. The mapping function $p(\cdot)$ reflects the relationship between the current state and the previous state, and $h(\cdot)$ is the mapping function between the measurement result and the state.

Gebraeel et al. [49] verified that the exponential model can effectively fit bearing damage. The DEM has better

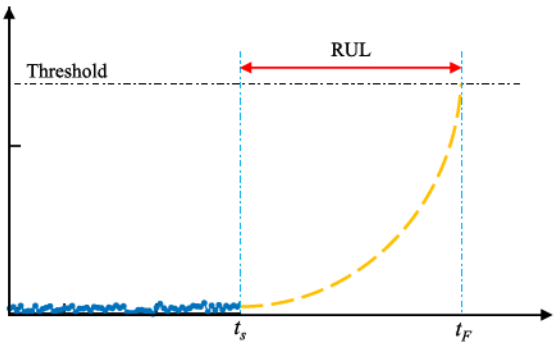

Fig. 5. Schematic of RUL prediction.

adaptability than the exponential model. At the same time, Peng et al. [24] applied the DEM to the fitting of engine degradation. To improve the applicability of the model, a DEM is used to predict the damage evolution of the bearing. The DEM is applied in the proposed algorithm to simulate the bearing degradation process. The expression is

$$y = a \times e^{bx} + c \times e^{qx} \tag{24}$$

where y is the RDIs of the bearing, x is the time, and a, b, c, q are the parameters of DEM. DEM is transformed into the following equation by using (22):

$$\begin{cases} a(k+1) = a(k) + N(0, \sigma_a) \\ b(k+1) = b(k) + N(0, \sigma_b) \\ c(k+1) = c(k) + N(0, \sigma_c) \\ q(k+1) = q(k) + N(0, \sigma_d). \end{cases} \tag{25}$$

The observation equation is also written as

$$y(k) = a(k) \cdot e^{b(k)\cdot k} + c(k) \cdot e^{q(k)\cdot k}. \tag{26}$$

The PF first generates initialized particles for tracking damage according to the prior distribution $p(x_0)$, and the particles weight $\omega_0^{(i)} = 1/N$. Then, the posterior distribution $p(x_k|y_{1:k})$ and the particle weight $\omega_k^{(i)}$ at time k are obtained from the Monte Carlo simulation. The particles and weights are updated by the sequential importance sampling (SIS) algorithm. The particles with small weights are discarded using the resampling method, and the number of particles with large weights is increased. After predicting, updating, calculating weights, and resampling, the particle iteration is completed. The model parameters are then estimated from the expectations of the output particles.

The data collected at the current time (t_s) is taken as input. DEM-based PF algorithm predicts the evolution of subsequent RDIs. The time when the predicted RDIs exceed the threshold is t_F. The RUL of the bearing is then calculated as: $t_{RUL} = t_F - t_s$. Fig. 5 is a schematic of the RUL prediction process.

B. Evaluation of RUL Prediction

To evaluate the effect of prediction, this article compares the prediction results of DEM-based PF, modified Paris model, and Gaussian process regression (GPR). In 1963, Paris and Erdogan [50] proposed a formula to describe the law of crack propagation and established the relationship between the fatigue crack growth rate and the stress intensity factor of the crack

$$\frac{da}{dN} = C(\Delta K)^m \tag{27}$$

where a is the crack length, N is the load cycle period, ΔK is the stress intensity factor, and C, m reflects the material parameters related to the mechanical properties of the material, which can be measured by experiments. In 2017, Qian et al. [31] modified the Paris model. When the Paris model is applied to the RUL prediction of bearings, it can be written in the following form:

$$N_{\text{RUL}} = N_{\text{th}} - N_i = \int_{l_i}^{l_{\text{th}}} \frac{da}{C(\Delta K)^m} \tag{28}$$

where N_{RUL} is the remaining life of the bearing, N_{th} is the time to reach the threshold, and N_i is the current working time. Rewrite (28) into integral form, the upper limit of integration l_{th} represents the crack length when the threshold is reached, and the lower limit $l_i$represents the crack length in the current state. For ball bearings, $\Delta K = \Delta\sigma(\pi a)^{1/2}$. $\Delta\sigma$ is the stress range. Meanwhile, the indicator proposed in this article has a linear relationship with the damage of the bearing, which is proven in Section II, $\text{DI} = c_t = kl$. Equation (28) can then be rewritten as

$$N_{\text{RUL}} = \int_{c_i}^{c_{\text{th}}} \frac{k^2 dc_t}{C\Delta\sigma\pi^{m/2}k^{m/2}c_t^{m/2}}. \tag{29}$$

For rolling bearings, m is usually taken as 2 and k, C, $\Delta\sigma$ are all constants; hence, the RUL of the bearing can be computed by

$$N_{\text{RUL}} = \int_{c_i}^{c_{\text{th}}} \frac{k}{C\Delta\sigma\pi} \frac{dc_t}{c_t} = A \ln \frac{c_{\text{th}}}{c_i} + B \tag{30}$$

where $A = k/(C\Delta\sigma\pi)$, and B is the integral constant. The RUL can be computed by (30) with known material parameters or empirical parameters.

GPR was successfully applied to RUL prediction of bearings [51]. GPR is a nonparametric model for data regression analysis. The definition of a Gaussian process consists of the following three steps:

$$f(x) \sim \text{GP}\big(m(x), k\big(x, x'\big)\big) \tag{31}$$

$$m(x) = E[f(x)] \tag{32}$$

$$k\big(x, x'\big) = E\big[\big(f(x) - m(x)\big)\big(f\big(x'\big) - m\big(x'\big)\big)\big] \tag{33}$$

where x is the collected data, $m(x)$ is the mean function, and $k(x,x')$ represents the covariance function. Equation (31) is used to determine the sampling points of the Gaussian process, (32) is used to calculate the mean function, and (33) is used to calculate the covariance function. Then, the expression of the prediction point is determined according to the posterior probability, the hyperparameter is solved by maximum likelihood estimation, and finally, the data are substituted into the prediction.

The relative error is used to describe the accuracy of the prediction, which is denoted as

$$A = 1 - \frac{|\text{RUL}^* - \text{RUL}|}{\text{RUL}} \times 100\% \tag{34}$$

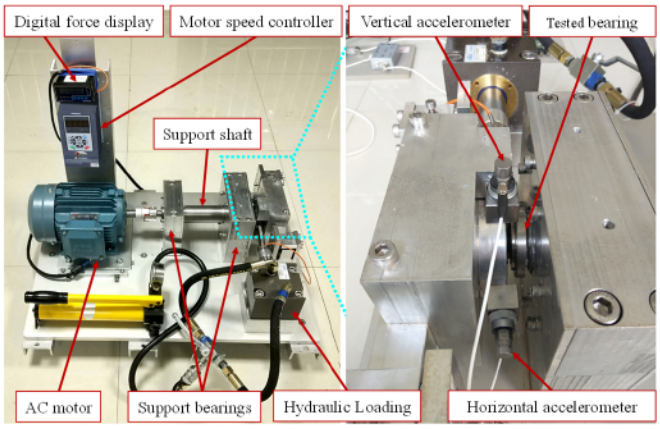

Fig. 6. Experimental platform of XJTU-SY [26].

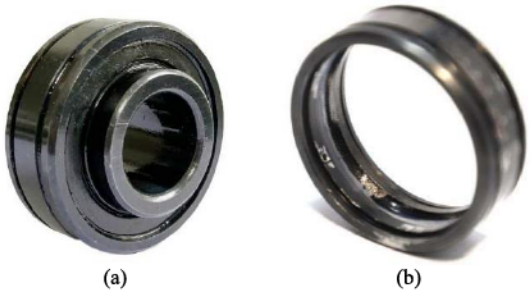

Fig. 7. (a) Healthy bearing. (b) Outer race wear.

where A is the prediction accuracy, RUL represents the true life of bearings, and RUL* is the predicted life.

IV. Experimental Demonstration

A. Case 1: Accelerated Degradation Test From XYTU-SY Bearing Datasets

To illustrate the effectiveness of the RUL prediction approach proposed in this article, a public dataset of run-to-failure signals from XJTU-SY bearing datasets is analyzed. The experimental platform is shown in Fig. 6 [26].

The bearing used in the test is LDK UER204. The rotation speed is 2400 r/min. The bearing is loaded at 10 kN, and the bearing has an outer race defect at the end of the test. The comparison between health and damaged bearings is shown in Fig. 7.

During the experiment, the vibration signals of the bearing were collected by acceleration sensors in both vertical and horizontal directions. The experimental platform was sampled every 1 min, the sampling frequency was 25.6 kHz, and the sampling time was 1.28 s. The data of bearing 3_1 is used in this experiment. The rotating frequency of the bearing is 40 Hz, and the load is 10 kN.

In the test, the bearing damage stage is tracked by SRPSW. The bearing runs smoothly in the early stage; hence, the sampling interval is increased. The sampling interval in the early stage was changed from 1 to 2 min. The sampling interval is restored to 1 min after reaching the normal stage

TABLE II
Parameters Used in PSW of Case 1

Parameters	m	d	nm	nb	nn	rl
Healthy stage	11	6	2^{16}	5	2^5	2^{15}
Degradation stage	13	6	2^{16}	10	2^5	2^{15}

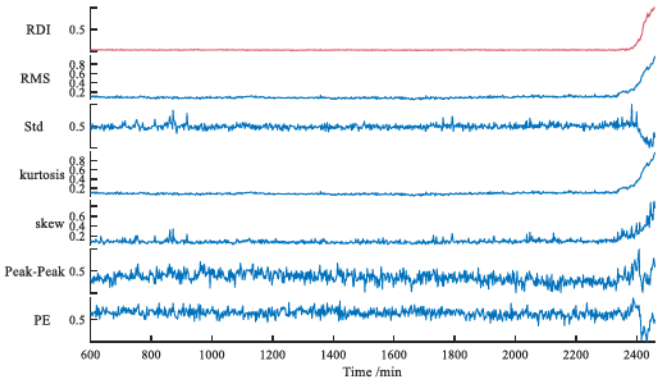

Fig. 8. Degradation curve of various indicators in Case 1.

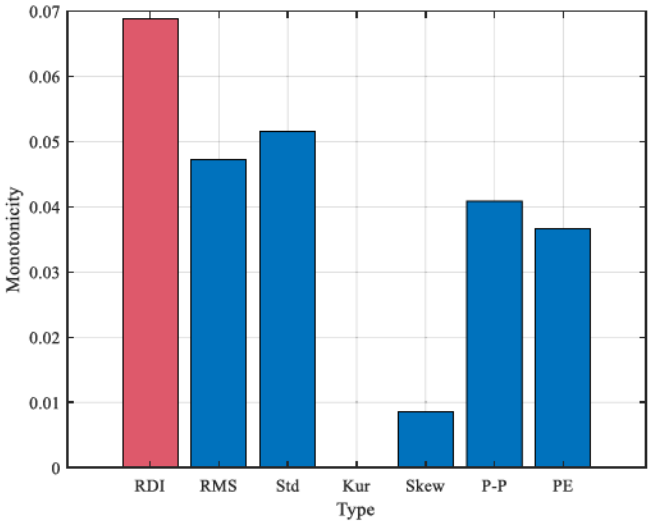

Fig. 9. Monotonicity criterion for different indicators in Case 1.

threshold to improve the RUL prediction accuracy. The collected vibration signal is processed by a low-pass filter and then embedded in the SRPSW. The parameters obtained by the mutual information method and false-nearest-neighbors method are shown in the first row of Table II.

In Table II, m is the time delay of the reconstructed phase space, d denotes the embedding dimension, nm represents the number of data points used in the construction of the reference phase space, nb is the number of subspaces, nn represents the number of nearest neighbors, and rl denotes the number of data points monitored in real time.

To demonstrate the advantages of the indicator proposed in this article, the PDIs in Table I are used for comparison. The same data length as the SRPSW is used to calculate the PDI value. All DIs are normalized, and the results are shown in Fig. 8. The monotonicity of the indicators is plotted in Fig. 9.

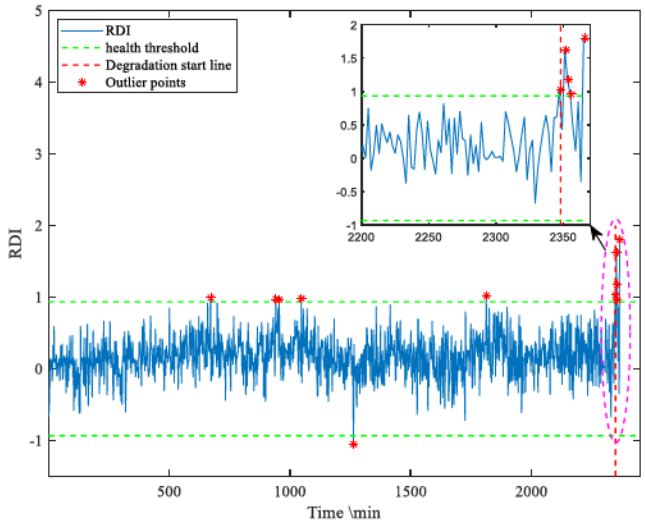

Fig. 10. RDIs of healthy stage in Case 1.

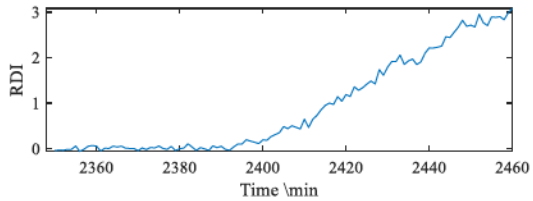

Fig. 11. RDIs of degradation stage in Case 1.

It can be seen from Fig. 8 that the RDI extracted by the SRPSW has less interference than other commonly used indicators. The monotonicity of the indicator quantitatively describes its ability to track damage, with greater monotonicity indicating a more consistent tracking effect. The results in Fig. 9 show that the proposed algorithm is better in tracking bearing damage.

To continue to analyze the results of SRPSW, the RDIs in the healthy stage obtained by SRPSW are shown in Fig. 10.

The harsh working conditions in Case 1 accelerate the degeneration and shorten the healthy stage of bearings. The sampling time interval in the experiment is adjusted to 2 min. To ensure the effectiveness of the 3σ interval and avoid wasting data, the first 15 data points (15×2 min $=$ 30 min) are used to compute μ and σ. The RDI for the first 30 min was used to estimate a bearing health threshold range $[-0.9336, 0.9336]$ (the green dotted line marks in Fig. 10). It can be seen from Fig. 10 that several outliers (red points) appeared in the healthy stage; however, these outliers do not meet the requirements and are excluded. The stage division requires three consecutive RDIs to exceed the threshold. Starting from the 2348th min, three consecutive points meet the requirements. Thus, the bearing enters the degradation stage after the 2350th min.

The parameters of the bearing in the degradation stage are recomputed and shown in the second row of Table II. Fig. 11 plots the RDIs in the degradation stage. Fig. 11 demonstrates that the RDIs fluctuate slightly at the beginning of the bearing degradation stage (2348–2390 min), which indicates that the RDIs are sensitive to the early damage. In the middle part of the bearing degradation stage (2390–2464 min), RDIs begins to rise, which indicates that the bearing has been slightly damaged.

TABLE III
INITIAL PARAMETERS OF THE PF IN CASE 1

a	b	c	q
-0.6847	0.054	0.6919	-0.1546

RDIs are used for real-time prediction after the bearing has run into the degradation stage. At the beginning of the degradation stage, minor faults do not affect the normal working of the bearing. However, the evolution of damage gradually jeopardizes the normal operation of the machine. Different machines have different tolerances for the degree of failure. As a result, a threshold needs to be set artificially. The range of RDIs for the healthy stage is $[-0.9336, 0.9336]$, which is used to compute the threshold for the degenerate stage. The upper limit of the range for the health stage is $T_{\mathrm{H1}} = 0.9336$. About three or four times, T_{H1} is taken as the threshold for the failure stage. The failure threshold of RDIs is set as $T_{\mathrm{F}} = 3$ in Case 1, and the degradation stage ends when the RDIs exceed T_{F}, after which, the bearings can be repaired or replaced to keep the machine running safely.

While extracting bearing RDIs, PF is used to predict future RDIs. A nonlinear function fitting method is applied to estimate the initial prior information of the DEM. The RDIs of the first 15 min are used to fit the initial state, and the updated initial parameters (a, b, c, q) of DEM are shown in Table III.

The moment of entering the degradation stage is set to zero, and the RUL prediction starts from the zero point. Since the life prediction is computed in real time, only the results of three moments (20th min, 60th min, and 100th min) are shown in Figs. 12–14. Fig. 12 shows the results at the 20th min, Fig. 13 plots the results at the 60th min, and Fig. 14 illustrates the results at the 100th min. The blue and red solid lines in the left subgraph of the Figs. 12–14 show the actual and estimated results of RDIs from the beginning to the current, and the green solid line is the predicted damage evolution curve. The four subgraphs on the right side of the figure represent the real-time prediction results of the parameters of the DEM.

Figs. 12–14 demonstrate that the estimated points obtained by the PF fit the actual RDIs and track the degradation process of the bearing. The right four subgraphs in each figure plot the four parameters (a, b, c, q) in the DEM. The right subgraph of Fig. 12 plots the variation of model parameters. The most suitable model parameters at each moment are given. The right subgraph of Fig. 13 shows small fluctuations of the estimated model parameters before the 43rd min, which indicates that the model is suitable. At the 43rd min, the four parameters of the model suddenly changed, indicating that the working state of the bearing has changed. The previous model was no longer suitable for the current RDI. Fig. 14 is the later stage of the bearing degradation. RDIs are tracked in the left subgraph, and the estimation of model parameter is tracked in the right subfigure. The RUL is predicted by iteratively updating the DEM parameters.

The results of RUL prediction are shown in Fig. 15(a), and RDIs of the degradation stage are added to Fig. 15(b)

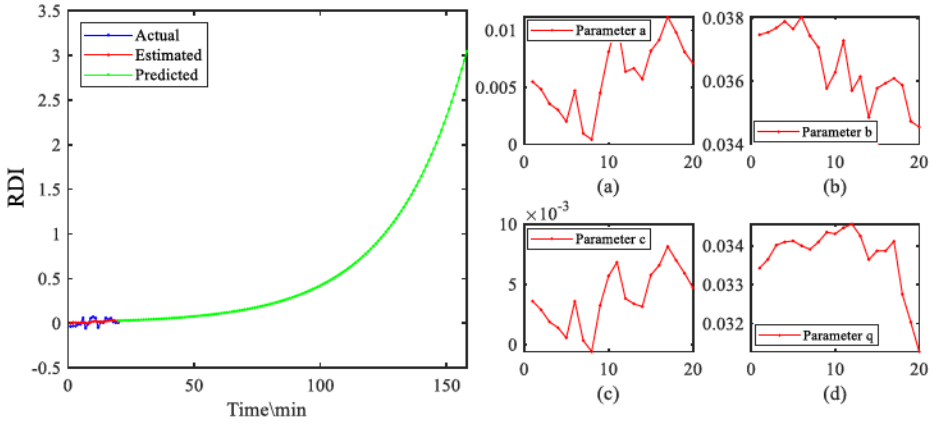

Fig. 12. PF result at 20 min.

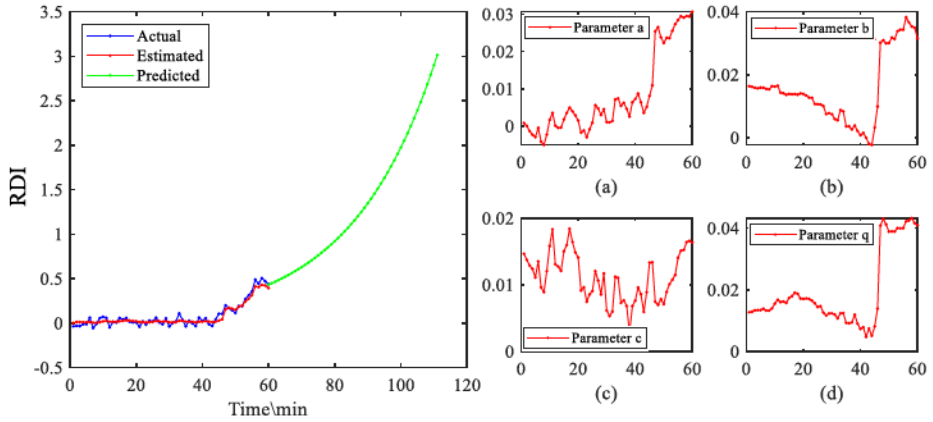

Fig. 13. PF result at 60 min.

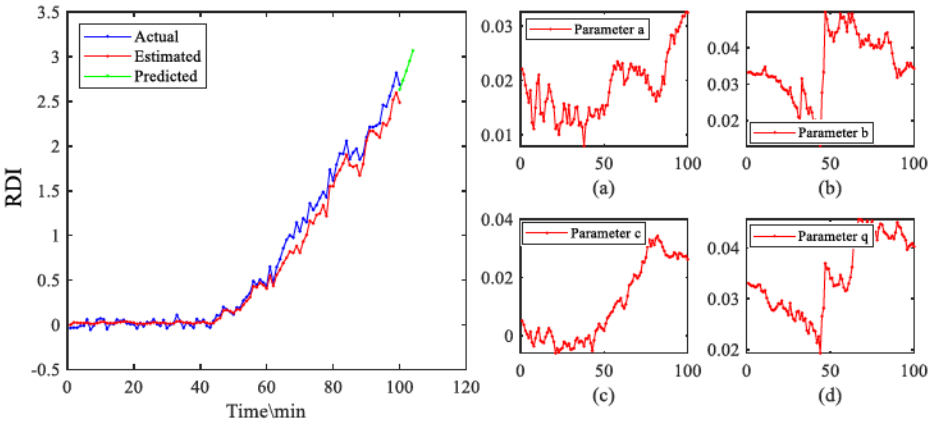

Fig. 14. PF result at 100 min.

for reference. Since the data of the first 15 min are used to estimate the initial state of the PF, the RUL of the first 15 min is removed from Fig. 15. From the start to the 19th min (point A), the predicted RUL drops from the 159th min to the 123rd min in that the data before point A is affected by initial conditions. RUL increased from 20 to 46 min (point B) and fluctuated between 220 and 334 min in virtue of the stable of RDIs during this time. The predicted RUL at the 46th min drops significantly, indicating abrupt degradation of the bearing. SRPSW predicts that the bearing enters the failure period at the 92nd min (point C), and RUL = 0. This result is consistent with the extracted RDIs, indicating that the proposed algorithm conforms to the law of bearing degradation.

The Paris model is used to compute the RUL on the same data, and the results of the Paris model are used as the comparison of the proposed algorithm. The Paris model requires a large number of material parameters. It is difficult

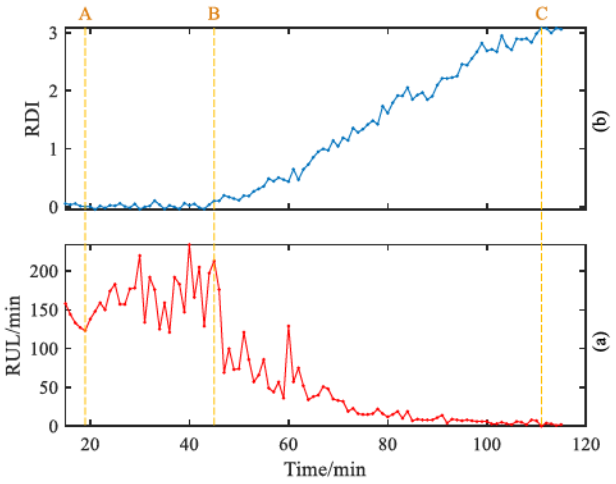

Fig. 15. Damage tracking and RUL prediction of Case 1. (a) RDIs. (b) RUL prediction.

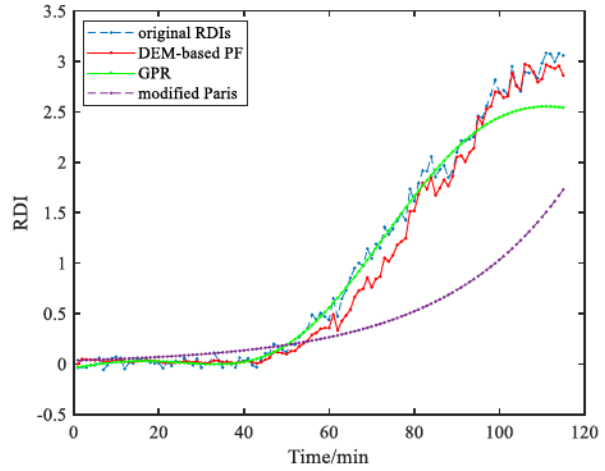

Fig. 16. Comparison of damage tracking results in Case 1.

to obtain an accurate value for the RUL of the bearing, and it is assumed in this article that the RUL decreases linearly. The RUL of the bearing at the start of prediction is 115 min, and the RUL is reduced to zero at the end of the prediction.

The damage tracking comparison of the three methods is shown in Fig. 16. In the later degradation stage, Paris model is ineffective in tracking the evolution of damage, and the accuracy of the GPR method is also insufficient. The proposed method tracks damage well both in the early and late stages.

The errors of the prediction results of the proposed approach after smoothing are shown in Fig. 17. It can be seen from Fig. 17 that the error of the predicted results decreases as the bearing damage evolves.

Equation (34) is used to compute the prediction accuracy of both methods. The prediction accuracy of the algorithms is shown in Table IV. The proposed algorithm is demonstrated to outperform the comparison method.

The XJTU-SY dataset is fully utilized to illustrate the effectiveness and superiority of the method. Three more experimental data were analyzed here. The computed accuracies from other degradation processes are displayed in Table V.

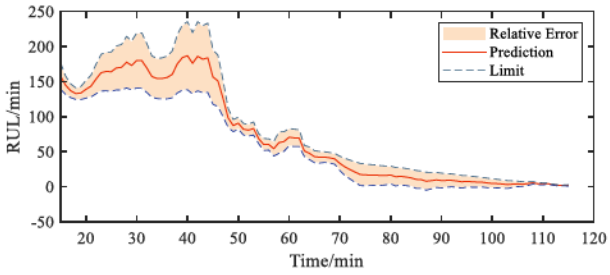

Fig. 17. Prediction error of Case 1.

TABLE IV
PREDICTION ACCURACY IN CASE 1

Algorithm	DEM-based PF	Paris model	GPR
Accuracy	90.16%	27.69%	89.27%

TABLE V
PREDICTION ACCURACY FOR DIFFERENT SAMPLES

Number	Accuracy	Parameters					
		m	*d*	*nm*	*nb*	*nn*	*rl*
3_2	91.27%	6	5	2^{16}	10	2^5	32768
3_3	90.56%	9	7	2^{16}	10	2^5	32768
3_4	90.63%	11	7	2^{16}	10	2^5	32768

It can be seen from Table V that the proposed approach has perfect generalization and accurately predicts the RUL for different degradation data.

In summary, SRPSW tracks the damage in the accelerated bearing degradation test in real time and predicts the RUL of the bearing. Comparison of the SRPSW with the commonly used statistical methods shows the accuracy and anti-interference of RDIs. Different parameters are used for the extraction of damage signals at different stages. The moment when the bearing enters the stage of damage degradation can be clearly identified. By comparison with the modified Paris model and GPR, DEM-based PF shows its advantages in RUL prediction. Since no material parameters are required, the prior information required by PF can be extracted from the earlier RDIs. The results of damage tracking and RUL prediction demonstrate the effectiveness of the proposed algorithm.

B. Case 2: Normal Degradation Test From Intelligent Maintenance Systems (IMS) Bearing Dataset

To further verify the effectiveness of the proposed algorithm, the data of NSF I/UCR Center are utilized for analysis [52], and the experimental platform is shown in Fig. 18. Four Rexnord ZA-2115 double row bearings were used in the test. The rotation speed is 2000 r/min. The load on the bearing is 6000 lbs. Accelerometers are used to collect the vibration signal of the bearing, the sampling frequency is 20 kHz, the sampling time is 1 s, and the sampling time interval is 20 min. The difference between Case 2 and Case 1 is that Case 2 is a run-to-failure test under normal conditions rather than an accelerated degradation test, which can better illustrate the performance of the proposed approach under actual conditions.

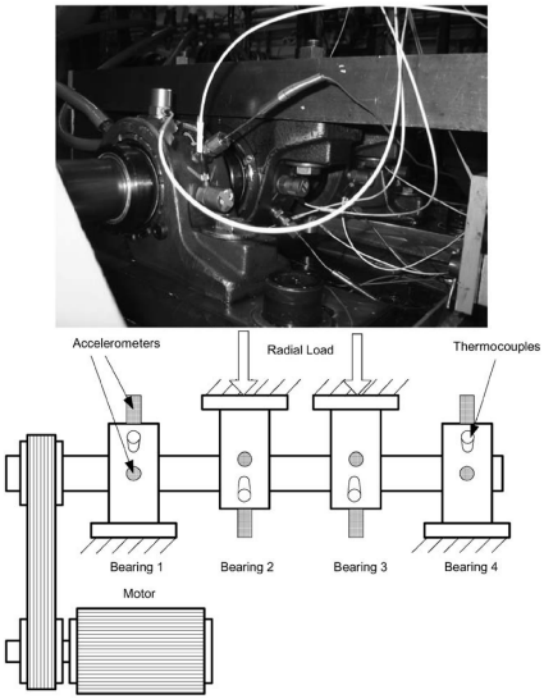

Fig. 18. Photograph and schematic of the platform in Case 2 [52].

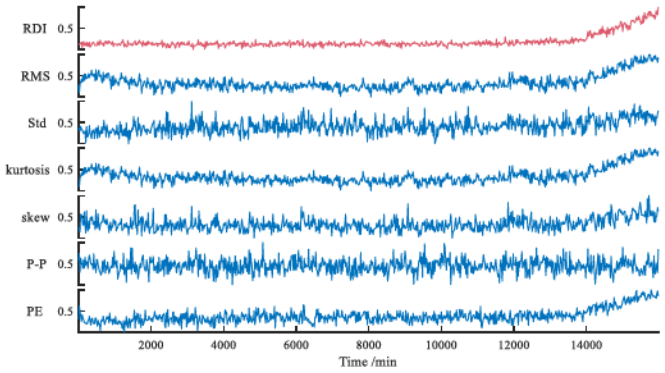

Fig. 19. Degradation curve of various indicators in Case 2.

TABLE VI
PARAMETERS USED IN PSW OF CASE 2

Parameters	m	d	nm	nb	nn	rl
Healthy stage	6	6	2^{15}	10	2^5	20480
Degradation stage	6	8	2^{15}	5	2^5	20480

The experiment started on February 12, 2004 and ended on December 19, 2004. Bearing 1 had an outer race defect.

The bearing vibration signal is first processed by a low-pass filter to remove the interference of high-frequency components, and then used for RDIs extraction. The parameters used in the healthy stage are shown in the first row of Table VI.

Similar to the process of Case 1, the RDIs are extracted from the damage matrix in the healthy stage: RDI, rms, Std, Kurtosis, Skew, and Peak–Peak. The normalized metrics are plotted in Fig. 19. Fig. 20 illustrates the monotonicity of these indicators. The analysis results show that the monotonicity of

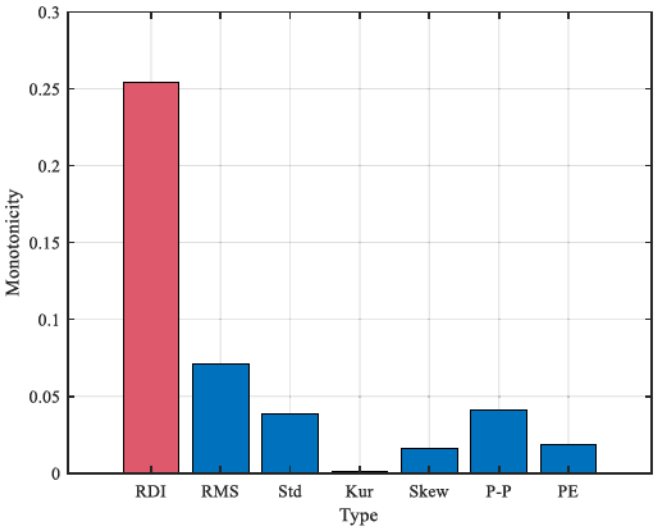

Fig. 20. Monotonicity criterion for different indicators in Case 2.

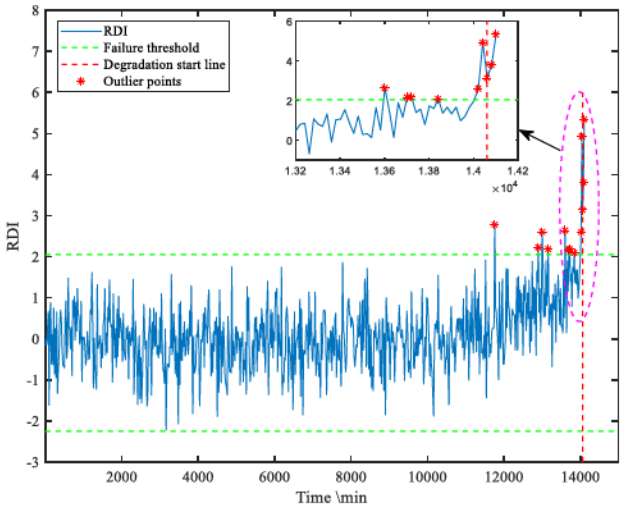

Fig. 21. RDIs of healthy stage in Case 2.

RDI is better. The obvious degradation curve can be extracted in the normal degradation test.

A more detailed RDI is presented in Fig. 21. The sampling time interval in Case 2 is 20 min, and the bearing runs under normal conditions. Since the time interval is long, the data length is appropriately reduced. The first ten points (10×20 min $= 200$ min) are used to compute the threshold range for the healthy stage. RDI of the first 200 min is used to compute the threshold for the bearing to enter the degradation stage. According to the 3σ principle, the range of the threshold for the healthy stage is $[-2.2447, 2.0562]$. The proposed algorithm considers that when more than three consecutive RDIs exceed the threshold, the bearing enters the degradation stage. It can be seen from Fig. 21 that there are a small number of outliers in the late healthy stage, but these outliers do not meet the judgment conditions. The point beyond the threshold is marked in Fig. 21, indicating that the bearing entered the degradation stage at the 140 60th min.

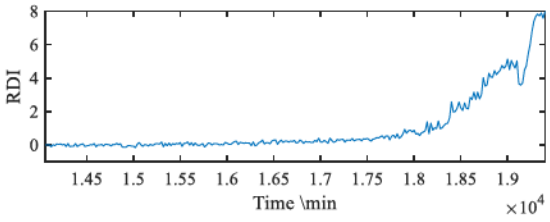

Fig. 22. RDIs of degradation stage in Case 2.

TABLE VII
INITIAL PARAMETERS OF THE PF IN CASE 2

a	b	c	q
6.829×10^{-3}	2.349×10^{-2}	-3.547×10^{-2}	-2.190×10^{-2}

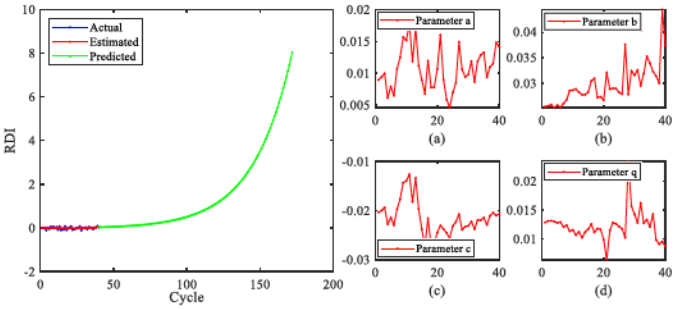

Fig. 23. PF result at cycle 40.

The parameters used in the degradation stage are shown in the second row of Table VI. The extracted RDIs are shown in Fig. 22. The upper limit of the range of the healthy stage is $T_{H1} = 2.0562$. The threshold for the degradation stage is four times T_{H1}. The bearing failure threshold $T_F = 8$. The indicator shows that the bearing entered the degradation stage from the 14060th min and reached the failure threshold at the 19400th min. RDI is relative value, and the RDIs in the degradation stage are not affected by the healthy stage. Thus, RDIs are smooth in the early stage of the degradation, which can improve the accuracy of damage tracking.

The RDIs of the degradation stage are extracted. PF is used to predict the RUL of the bearing. The first ten RDIs of the degradation stage are used for the fitting of the initial state. The initial parameters of the DEM are shown in Table VII.

The sampling interval of the experiment is 20 min. Therefore, 20 min was taken in a cycle. The following three figures show the RUL prediction, and model parameter estimation results at the 800th min, 3000th min, and 5200th min in the degradation stage. The four subplots to the right of each figure plot the variation of the four parameters (a, b, c, q) in the DEM with cycles.

Fig. 23 shows the results of the 40th cycles in the degradation stage. It can be seen from the left subgraph that the estimated RDIs are consistent with the actual RDIs. The model parameters displayed in the right subgraph do not fluctuate greatly. At the 150th cycle (Fig. 24), the estimated RDIs show an increasing trend, and the predicted RDIs gradually approached the real RDIs. The model parameters on the right subgraph changes abruptly around the 50th and 100th cycles.

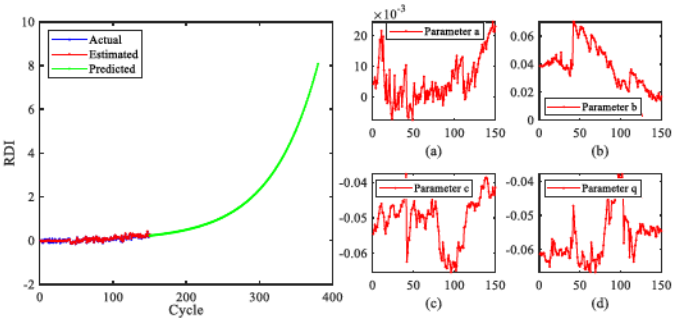

Fig. 24. PF result at cycle 150.

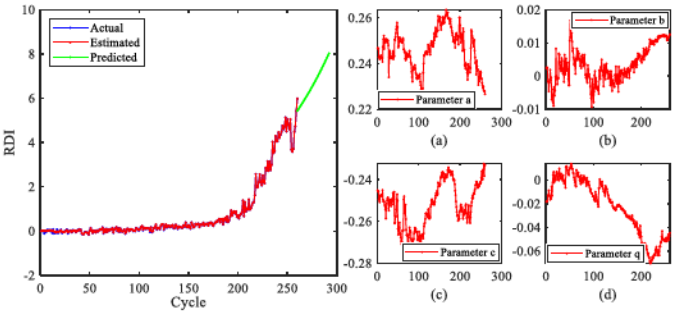

Fig. 25. PF result at cycle 260.

TABLE VIII
PREDICTION ACCURACY IN CASE 2

Algorithm	DEM-based PF	Paris model	GPR
Accuracy	90.78%	65.30%	85.37%

At the 260th cycle (Fig. 25), the prediction of the RDIs in the left subgraph is close to the threshold. The model parameters in the right subgraph have a suddenly change around 200 cycles, indicating that the bearing state has changed. At the same time as RDIs tracking, RUL prediction is monitored in real time.

Fig. 26 plots the results of RDIs and RUL. It can be seen from Fig. 26 that the RUL fluctuates in the range of 200 cycles (4000 min) to 400 cycles (8000 min) in the early and middle of the degradation stage. The RUL began to drop at the 3560th min (point A), indicating that the bearing is about to enter the failure stage. After the 4120th min (point B), the prediction of RUL begins to decrease continuously until the bearing fails.

The damage tracking curves of the three methods are plotted in Fig. 27. It can be seen from Fig. 27 that DEM-based PF has a better effect on damage tracking.

The relative error after smoothing is plotted in Fig. 28. The curve in Fig. 28 reflects the change of the relative error value at different times under general working conditions. Although the error is larger at some points, most of the prediction points of the proposed algorithm ensure the prediction accuracy.

Same as Case 1, (34) is used to analyze the prediction accuracy of RUL of the proposed approach. The prediction accuracy of the algorithms is shown in Table VIII. Obviously, the proposed algorithm is more accurate.

The run-to-failure test under normal conditions in this section is used to verify the effectiveness of the proposed

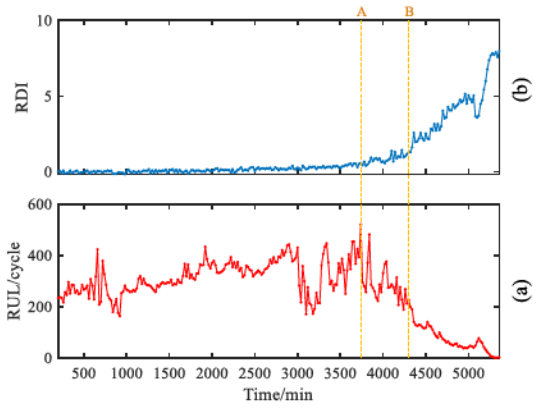

Fig. 26. Damage tracking and RUL prediction of Case 2. (a) RDIs. (b) RUL prediction.

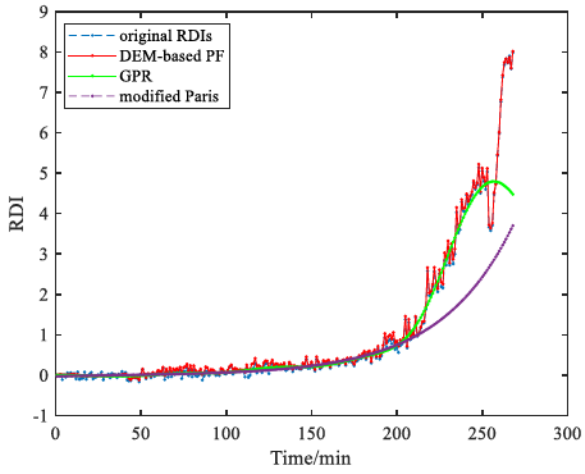

Fig. 27. Comparison of damage tracking results in Case 2.

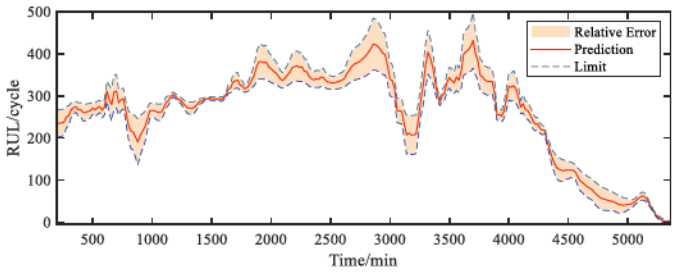

Fig. 28. Prediction error of Case 2.

approach. Under normal working conditions, the RDI extracted by SRPSW is more accurate. Thus, SRPSW extracts the RDIs of the bearing and divides the working stage reasonably. The proposed approach avoids the failure of the reference phase space in the original PSW. The results compared with the Paris model and GPR demonstrate that DEM-based PF is more accurate, and it does not require material parameters, which improves the practicality. The RUL prediction results illustrate that the proposed method is promising in mechanical maintenance.

V. Conclusion

In this article, an SRPSW algorithm is proposed to track damage. Based on nonlinear dynamics, SRPSW algorithm extracts bearing damage segmentally. SRPSW eliminates the shortage of the original PSW when the predicted faults exceed the reference phase space in the bearing prognostic. During the RUL prediction, the PF based on DEM avoids the requirement of material parameters in the physical model. The reliability of the proposed approach has been verified by accelerated degradation test and normal degradation test. RDIs extracted from SRPSW are compared with widely used indicators. RDIs outperform other indicators in tracking bearing damage. Further, the prediction accuracy of DEM-based PF is compared with the improved Paris model and GPR. The experimental results show that the prediction accuracy of the proposed approach is outstanding. For unknown machinery, the subjectively chosen threshold influences the prediction accuracy. Adaptive thresholds will be addressed in future research.

References

[1] A. Heng, S. Zhang, A. C. C. Tan, and J. Mathew, "Rotating machinery prognostics: State of the art, challenges and opportunities," *Mech. Syst. Signal Process.*, vol. 23, no. 3, pp. 724–739, 2009.

[2] H. Zhao, H. Liu, J. Xu, and W. Deng, "Performance prediction using high-order differential mathematical morphology gradient spectrum entropy and extreme learning machine," *IEEE Trans. Instrum. Meas.*, vol. 69, no. 7, pp. 4165–4172, Jul. 2020.

[3] B. Chen et al., "Integrated early fault diagnosis method based on direct fast iterative filtering decomposition and effective weighted sparseness kurtosis to rolling bearings," *Mech. Syst. Signal Process.*, vol. 171, May 2022, Art. no. 108897.

[4] S. Lv, Y. Lv, R. Yuan, and H. Li, "High-order synchroextracting transform for characterizing signals with strong AM-FM features and its application in mechanical fault diagnosis," *Mech. Syst. Signal Process.*, vol. 172, Jun. 2022, Art. no. 108959.

[5] Y. Wang, Y. Peng, Y. Zi, X. Jin, and K. L. Tsui, "A two-stage data-driven-based prognostic approach for bearing degradation problem," *IEEE Trans. Ind. Informat.*, vol. 12, no. 3, pp. 924–932, Jun. 2016.

[6] Y. Lei, J. Lin, Z. He, and M. J. Zuo, "A review on empirical mode decomposition in fault diagnosis of rotating machinery," *Mech. Syst. Signal Process.*, vol. 35, nos. 1–2, pp. 108–126, Feb. 2013.

[7] Y. Lv, R. Yuan, and G. Song, "Multivariate empirical mode decomposition and its application to fault diagnosis of rolling bearing," *Mech. Syst. Signal Process.*, vol. 81, pp. 219–234, Dec. 2016.

[8] L. Song, P. Chen, and H. Wang, "Vibration-based intelligent fault diagnosis for roller bearings in low-speed rotating machinery," *IEEE Trans. Instrum. Meas.*, vol. 67, no. 8, pp. 1887–1899, Aug. 2018.

[9] B. Chen et al., "Fault diagnosis method based on integration of RSSD and wavelet transform to rolling bearing," *Measurement*, vol. 131, pp. 400–411, Jan. 2019.

[10] Y. Ma, Y. Lv, R. Yuan, and G. Song, "Matching synchroextracting transform for mechanical fault diagnosis under variable-speed conditions," *IEEE Trans. Instrum. Meas.*, vol. 71, pp. 1–12, 2022.

[11] E. El-Thalji and E. Jantunen, "A summary of fault modelling and predictive health monitoring of rolling element bearings," *Mech. Syst. Signal Process.*, vols. 60–61, pp. 252–272, Aug. 2015.

[12] M. S. Kan, A. C. C. Tan, and J. Mathew, "A review on prognostic techniques for non-stationary and non-linear rotating systems," *Mech. Syst. Signal Process.*, vols. 62–63, pp. 1–20, Oct. 2015.

[13] Y. Lei, N. Li, L. Guo, N. Li, T. Yan, and J. Lin, "Machinery health prognostics: A systematic review from data acquisition to RUL prediction," *Mech. Syst. Signal Process.*, vol. 104, pp. 799–834, May 2018.

[14] R. Yuan, Y. Lv, Q. Kong, and G. Song, "Percussion-based bolt looseness monitoring using intrinsic multiscale entropy analysis and BP neural network," *Smart Mater. Struct.*, vol. 28, no. 12, Oct. 2019, Art. no. 125001.

[15] D. Mba and R. B. K. N. Rao, "Development of acoustic emission technology for condition monitoring and diagnosis of rotating machines: Bearings, pumps, gearboxes, engines, and rotating structures," *Shock Vib. Dig.*, vol. 38, no. 1, pp. 3–16, 2006.

[16] P. Guo, D. Infield, and X. Yang, "Wind turbine generator condition-monitoring using temperature trend analysis," *IEEE Trans. Sustain. Energy*, vol. 3, no. 1, pp. 124–133, Jan. 2012.

[17] K. Manoj, M. ParbotiShankar, and M. N. Mohan, "Advancement and current status of wear debris analysis for machine condition monitoring: A review," *Ind. Lubrication Tribol.*, vol. 65, no. 1, pp. 3–11, Feb. 2013.
[18] D. Han, J. Yu, M. Gong, Y. Song, and L. Tian, "A remaining useful life prediction approach based on low-frequency current data for bearings in spacecraft," *IEEE Sensors J.*, vol. 21, no. 17, pp. 18978–18989, Sep. 2021.
[19] E. Jantunen, J. Hooghoudt, Y. Yang, and M. McKay, "Predicting the remaining useful life of rolling element bearings," presented at the IEEE Int. Conf. Ind. Tech., Lyon, France, Feb. 2018.
[20] N. Li, Y. Lei, J. Lin, and S. X. Ding, "An improved exponential model for predicting remaining useful life of rolling element bearings," *IEEE Trans. Ind. Electron.*, vol. 62, no. 12, pp. 7762–7773, Dec. 2015.
[21] S. Zhang, Y. Zhang, L. Li, S. Wang, and Y. Xiao, "An effective health indicator for rolling elements bearing based on data space occupancy," *Struct. Health Monitor.*, vol. 17, no. 1, pp. 3–14, Jan. 2018.
[22] L. Saidi, J. B. Ali, E. Bechhoefer, and M. Benbouzid, "Wind turbine high-speed shaft bearings health prognosis through a spectral Kurtosis-derived indices and SVR," *Appl. Acoust.*, vol. 120, pp. 1–8, May 2017.
[23] Z. Que, X. Jin, and Z. Xu, "Remaining useful life prediction for bearings based on a gated recurrent unit," *IEEE Trans. Instrum. Meas.*, vol. 70, 2021, Art. no. 3511411.
[24] K. Peng, R. Jiao, J. Dong, and Y. Pi, "A deep belief network based health indicator construction and remaining useful life prediction using improved particle filter," *Neurocomputing*, vol. 361, pp. 19–28, Oct. 2019.
[25] Z. Pan, Z. Meng, Z. Chen, W. Gao, and Y. Shi, "A two-stage method based on extreme learning machine for predicting the remaining useful life of rolling-element bearings," *Mech. Syst. Signal Process.*, vol. 144, Oct. 2020, Art. no. 106899.
[26] B. Wang, Y. G. Lei, and N. Li, "A hybrid prognostics approach for estimating remaining useful life of rolling element bearings," *IEEE Trans. Rel.*, vol. 69, no. 1, pp. 401–412, Mar. 2018.
[27] Y. Pan, J. Chen, and X. Li, "Bearing performance degradation assessment based on lifting wavelet packet decomposition and fuzzy C-means," *Mech. Syst. Signal Process.*, vol. 24, no. 2, pp. 559–566, 2010.
[28] D. Chelidze and M. Liu, "Dynamical systems approach to fatigue damage identification," *J. Sound Vib.*, vol. 281, nos. 3–5, pp. 887–904, Mar. 2005.
[29] D. Chelidze and J. P. Cusumano, "Phase space warping: Nonlinear time-series analysis for slowly drifting systems," *Philos. Trans. Roy. Soc. A, Math., Phys. Eng. Sci.*, vol. 364, no. 1846, pp. 2495–2513, Sep. 2006.
[30] P. Luo, N. Hu, L. Zhang, J. Shen, and Z. Cheng, "Improved phase space warping method for degradation tracking of rotating machinery under variable working conditions," *Mech. Syst. Signal Process.*, vol. 157, Aug. 2021, Art. no. 107696.
[31] Y. Qian, R. Yan, and R. X. Gao, "A multi-time scale approach to remaining useful life prediction in rolling bearing," *Mech. Syst. Signal Process.*, vol. 83, pp. 549–567, Jan. 2017.
[32] D. An, J.-H. Choi, and N. H. Kim, "Prognostics 101: A tutorial for particle filter-based prognostics algorithm using MATLAB," *Rel. Eng. Syst. Saf.*, vol. 115, pp. 161–169, Jul. 2013.
[33] H. Zhao, H. Liu, Y. Jin, X. Dang, and W. Deng, "Feature extraction for data-driven remaining useful life prediction of rolling bearings," *IEEE Trans. Instrum. Meas.*, vol. 70, pp. 1–10, 2021.
[34] C. Chen, B. Zhang, G. Vachtsevanos, and M. Orchard, "Machine condition prediction based on adaptive neuro–fuzzy and high-order particle filtering," *IEEE Trans. Ind. Electron.*, vol. 58, no. 9, pp. 4353–4364, Sep. 2011.
[35] H. Yan, Y. Qin, S. Xiang, Y. Wang, and H. Chen, "Long-term gear life prediction based on ordered neurons LSTM neural networks," *Measurement*, vol. 165, Dec. 2020, Art. no. 108205.
[36] B. Wang, Y. Lei, N. Li, and T. Yan, "Deep separable convolutional network for remaining useful life prediction of machinery," *Mech. Syst. Signal Process.*, vol. 134, Dec. 2019, Art. no. 106330.
[37] G. Wang and J. Xiang, "Remain useful life prediction of rolling bearings based on exponential model optimized by gradient method," *Measurement*, vol. 176, May 2021, Art. no. 109161.
[38] J. Wang and R. X. Gao, "Multiple model particle filtering for bearing life prognosis," in *Proc. IEEE Conf. Prognostics Health Manage. (PHM)*, Gaithersburg, MD, USA, Jun. 2013, pp. 1–6.
[39] H.-W.-X. Li, G. Lyngdoh, S. Doner, R. Yuan, and D. Chelidze, "Experimental monitoring and modeling of fatigue damage for 3D-printed polymeric beams under irregular loading," *Int. J. Mech. Sci.*, vol. 233, Nov. 2022, Art. no. 107626.
[40] F. Takens, "Detecting strange attractors in turbulence," in *Dynamical Systems and Turbulence, Warwick 1980*. Berlin, Germany: Springer, 1981, pp. 366–381.
[41] M. B. Kennel, R. Brown, and H. D. I. Abarbanel, "Determining embedding dimension for phase-space reconstruction using a geometrical construction," *Phys. Rev. A, Gen. Phys.*, vol. 45, no. 6, pp. 3403–3411, Mar. 1992.
[42] A. M. Fraser and H. L. Swinney, "Independent coordinates for strange attractors from mutual information," *Phys. Rev. A, Gen. Phys.*, vol. 33, no. 2, pp. 1134–1140, Feb. 1986.
[43] J. P. Cusumano and A. Chatterjee, "A dynamical systems approach to damage evolution tracking, Part 1: Description and experimental application," *J. Vib. Acoust.*, vol. 124, no. 2, pp. 250–257, 2002.
[44] S. H. Nguyen and D. Chelidze, "New invariant measures to track slow parameter drifts in fast dynamical systems," *Nonlinear Dyn.*, vol. 79, no. 2, pp. 1207–1216, Oct. 2014.
[45] J. Coble and J. Hines, "Identifying optimal prognostic parameters from data: A genetic algorithms approach," in *Proc. Annu. Conf. PHM Soc.*, San Diego, CA, USA, Sep. 2009, pp. 1–11.
[46] F. Yang, M. S. Habibullah, T. Zhang, Z. Xu, P. Lim, and S. Nadarajan, "Health index-based prognostics for remaining useful life predictions in electrical machines," *IEEE Trans. Ind. Electron.*, vol. 63, no. 4, pp. 2633–2644, Apr. 2016.
[47] S. Gao, X. Xiong, Y. Zhou, and J. Zhang, "Bearing remaining useful life prediction based on a scaled health indicator and a LSTM model with attention mechanism," *Machines*, vol. 9, no. 10, p. 238, Oct. 2021.
[48] J. Liu, W. Wang, F. Ma, Y. B. Yang, and C. S. Yang, "A data-model-fusion prognostic framework for dynamic system state forecasting," *Eng. Appl. Artif. Intell.*, vol. 25, pp. 814–823, Jun. 2012.
[49] N. Gebraeel, M. Lawley, R. Liu, and V. Parmeshwaran, "Residual life predictions from vibration-based degradation signals: A neural network approach," *IEEE Trans. Ind. Electron.*, vol. 51, no. 3, pp. 694–700, Jun. 2004.
[50] P. Paris and F. Erdogan, "A critical analysis of crack propagation laws," *ASME J. Basic Eng.*, vol. 85, no. 4, pp. 528–533, 1963.
[51] P. S. Kumar, L. A. Kumaraswamidhas, and S. K. Laha, "Selection of efficient degradation features for rolling element bearing prognosis using Gaussian process regression method," *ISA Trans.*, vol. 112, pp. 386–401, Jun. 2021.
[52] H. Qiu, J. Lee, J. Lin, and G. Yu, "Wavelet filter-based weak signature detection method and its application on rolling element bearing prognostics," *J. Sound Vib.*, vol. 289, nos. 4–5, pp. 1066–1090, 2006.

Hengyu Liu received the B.S. degree in mechanical engineering from the Department of Mechanical Engineering, Wuhan University of Science and Technology, Wuhan, China, in 2020, where he is currently pursuing the Ph.D. degree in mechanical engineering.

His research interests include prognostics and health management, fault detection and isolation, structure health monitoring, and nonlinear signal processing.

Rui Yuan (Member, IEEE) received the B.S. and Ph.D. degrees in mechanical engineering from the Department of Mechanical Engineering, Wuhan University of Science and Technology, Wuhan, China, in 2014 and 2019, respectively, under the supervision of Prof. Yong Lv.

From 2016 to 2017, he was a Visiting Scholar with the Nonlinear Dynamics Laboratory, University of Rhode Island, Kingston, RI, USA, under the supervision of Prof. David Chelidze. He is currently a Lecturer with the School of Machinery and Automation, Wuhan University of Science and Technology. He has authored over 30 peer-reviewed journal articles, including in *Mechanical Systems and Signal Processing* (MSSP), *Structural Health Monitoring* (SHM), and IEEE TRANSACTIONS ON INSTRUMENTATION AND MEASUREMENT (TIM). His research interests include fault detection and isolation, prognostics and health management, structural health monitoring, and nonlinear dynamics.

Yong Lv received the B.S. and M.S. degrees from the Department of Mechanical Engineering, Wuhan University of Science and Technology, Wuhan, China, in 1998 and 2000, respectively, and the Ph.D. degree from the University of Science and Technology Beijing, Beijing, China, in 2004.

He is currently a Full Professor with the School of Machinery and Automation, Wuhan University of Science and Technology. He has authored over 100 peer-reviewed journal articles, including in *Mechanical Systems and Signal Processing* (MSSP), *Structural Health Monitoring* (SHM), IEEE TRANSACTIONS ON INSTRUMENTATION AND MEASUREMENT (TIM), and *Measurement*. He has hosted three National Natural Science Foundations of China and over 30 projects in the fields of machinery dynamics and condition monitoring. His research interests include fault detection and isolation, prognostics and health management, structural health monitoring, and nonlinear dynamics.

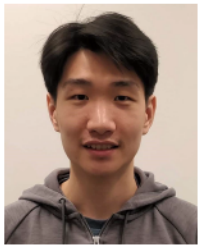

Hewenxuan Li received the Ph.D. degree in mechanical engineering and applied mechanics from the University of Rhode Island, Kingston, RI, USA, in 2022.

His research dedicates to the sensing, awareness, modeling, and prognosis of faults and damages in nonlinear systems. His research interests include but are not limited to fatigue damage identification, monitoring, and life estimation for nonlinear structures; multilength-scale and multitemporal-scale simulations and machine learning-based predictive modeling; and modal analysis of spatiotemporal fields and complex phenomena.

Ersegun Deniz Gedikli received the B.S. degree from the Department of Naval Architecture and Marine Engineering, Yildiz Technical University, Istanbul, Turkey, in 2010, and the M.S. and Ph.D. degrees from the Department of Ocean Engineering, University of Rhode Island, Kingston, RI, USA, in 2014 and 2017, respectively.

From 2017 to 2020, he was a Post-Doctoral Fellow at the Norwegian University of Science and Technology, Trondheim, Norway, where he worked on various offshore renewable energy and Arctic engineering projects. He is currently the Director of the Fluid-Structure Interactions and Nonlinear Dynamics Laboratory and an Assistant Professor with the Department of Ocean and Resources Engineering, University of Hawaii at Manoa, Honolulu, HI, USA. His research interests include experimental fluid-ice structure interactions, nonlinear dynamics, data science, flow-induced vibrations, Arctic offshore structures and marine operations, and offshore renewable energy systems.

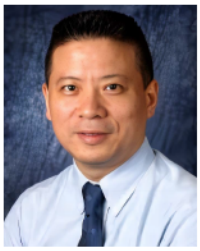

Gangbing Song (Member, IEEE) received the B.S. degree from Zhejiang University, Hangzhou, China, in 1989, and the M.S. and Ph.D. degrees from the Department of Mechanical Engineering, Columbia University, New York, NY, USA, in 1991 and 1995, respectively.

He is currently the Founding Director of the Smart Materials and Structures Laboratory and a Professor of Mechanical Engineering, Civil and Environmental Engineering, and Electrical and Computer Engineering with the University of Houston, Houston, TX, USA. He has developed two new courses in smart materials and authored over 400 articles, including over 200 peer-reviewed journal articles. He has expertise in smart materials and structures, structural vibration control, piezoceramics, ultrasonic transducers, structural health monitoring, and damage detection.

Dr. Song was a recipient of the NSF CAREER Award in 2001.